ELSEVIER

On the secondary stability of coated cementless hip replacement: parameters that affected interface strength

Julia Orlik [b], Alexei Zhurov [a,*], John Middleton [a]

[a] *UWCM, Biomechanics Research Unit, 27 Cardiff Medicentre, Cardiff CF14 4UJ, UK*
[b] *Fraunhofer Institut Techno- und Wirtschaftsmathematik, Gottlieb-Daimler-Strasse, Geb. 49, D-67663 Kaiserslautern, Germany*

Abstract

Unlike primary stability of coated cementless implants, their secondary stability has been poorly studied. This paper considers some theoretical aspects of the secondary stability of a coated cementless hip implant in a human femur. The bone is separated from the implant by a thin layer of microscopic peaks and troughs formed on the surface of the coating. The size of the peaks and troughs is very small compared with the macrosize of the implant stem and bone in contact. The study of the bone–stem contact by direct application of the finite element method is prohibitively costly. A two-scale asymptotic homogenisation procedure that takes into account the microgeometry of the interface layer and mechanical properties of bone and the implant material is applied to obtain effective, homogenised contact parameters. These parameters can be used in finite element analyses involving smooth interfaces, which require hundreds of times fewer finite elements. With the homogenisation technique and finite element analyses for a simplified design, two parameters were found to be most important—the normal contact stiffness and the friction coefficient. They both increase several times as bone grows into the rough surface of the implant and mineralises, thus providing a stronger interface and resulting in reduced micromotions.
© 2003 IPEM. Published by Elsevier Ltd. All rights reserved.

1. Introduction

Treatment for hip osteoarthritis focuses on decreasing pain and improving joint movement. When conservative methods of treatment fail, it is necessary to replace the affected joint with an artificial replacement prosthesis. Of the two types of hip prosthesis, cemented and cementless, the cementless hip prosthesis represents today approximately 35% of the European market and is regarded as more promising. The surface of the cementless implant is coated in such a way that the bone is in direct contact with this surface with the idea that the bone grows into the micro-troughs and pores of the coating to provide enhanced stability and rapid osseointegration.

It is well known that the primary stability of cementless stems is the key biomechanical factor determining the overall stability of the implant. The majority of authors agree that the implant mobility is the most important biomechanical cause for aseptic loosening of implants; e.g., see Refs. [1–4]. The stem stability is measured by the relative micromotion at the bone–implant interface. Once the primary stability has been achieved, due to the implant design and initial press-fit, bone remodelling processes are initiated, resulting eventually in additional, secondary stability, provided that the relative micromotions do not exceed a threshold value of about 200 μm and the stress field is nondestructive and other than zero. For experimental studies of the bone–implant interface structure and bone remodelling under various conditions, e.g., see Refs. [5–12].

The aim of the present paper is to take into account the effect of secondary stability and establish the macro-contact parameters that allow the replacement of the micro-rough bone–implant interface by a smooth one at the expense of a slight decrease in the accuracy of the

* Corresponding author. Tel.: +44-29-2068-2162.
E-mail address: zhurovai@cardiff.ac.uk (A. Zhurov).

results predicted. These parameters should take into account the microgeometry of the interface and mechanical properties of the contacting materials. To achieve this aim, we use an asymptotic homogenisation procedure based on the results of Refs. [13,14] and the approach of Refs. [15–17] extended to elastic contact problems and also numerically analyse a model design by the finite element method.

For mathematical treatment, the following assumptions are made: (i) the problem is linear elastic; (ii) the bone and implant materials are homogeneous; (iii) the implant is much stiffer than bone; (iv) the usual contact conditions at the interface are adopted: the contact surfaces do not penetrate each other and the normal stress is continuous and can only be compressive or zero; (v) Coulomb's friction law is adopted: as long as the absolute value of the shear stress at the contact boundary is less than the friction coefficient times the normal stress, the shear displacement at the interface is continuous; as soon as the equality is attained, a jump in the shear displacement arises which is proportional to the shear stress with some coefficient; and (vi) there is a small parameter, ε, the ratio of the characteristic dimension of the interface irregularities to the characteristic length of the bone–implant interaction zone, which allows applying an asymptotic homogenisation procedure.

Fig. 1 shows the typical surface microgeometry of a coated stem. The optimum range of pore sizes (average distances between major peaks and average peak heights) is reported (e.g., see Refs. [24]) to be between 100 and 400 μm.

2. Mathematical methods

Below, provided in brief, is the mathematical statement of the problem in the strong and variational formulations, as well as basic notation, methods employed, and main results. A detailed mathematical consideration will be given elsewhere.

2.1. Strong formulation

Two contacting domains are considered, D^ε (implant) and Ω^ε (bone), as schematically shown in Fig. 2. Although a 2D case is considered for simplicity, it can easily be extended to 3D. The right part of the boundary of D^ε is assumed to have a pattern represented by peaks arranged periodically with period εY_0, where ε is a small parameter and Y_0 is a characteristic length of the interaction zone. The domain Ω^ε is in contact with D^ε at the peaks. Formally we assume that Ω^ε is a Lipschitz domain in the 3D Euclidean space. We also introduce fixed domains $\Omega \subset \Omega^\varepsilon$ and $D \subset D^\varepsilon$ with plane boundaries, so that $(\Omega^\varepsilon \cup D^\varepsilon)\backslash(\Omega \cup D) \subset \Pi^\varepsilon$, where Π^ε is the thin layer
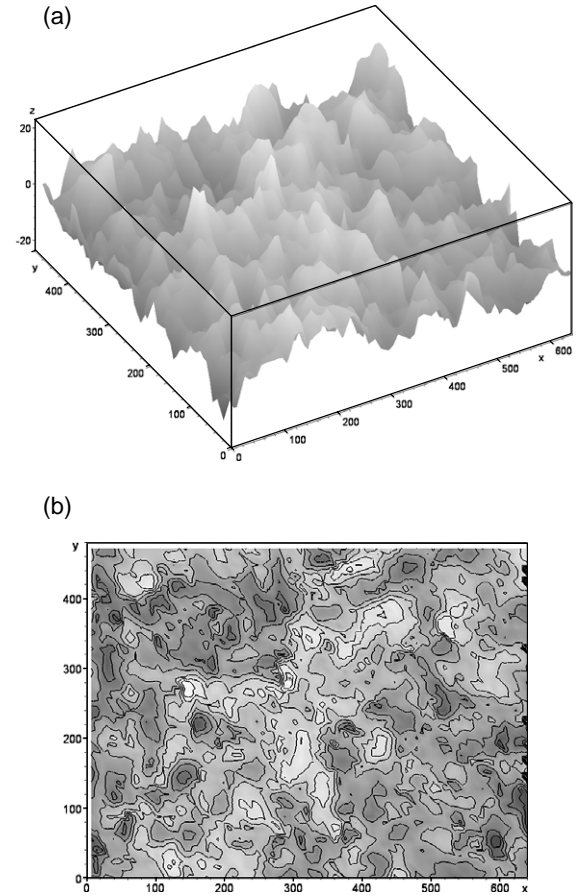

Fig. 1. Typical surface microgeometry of a coated stem: (a) isometric view of a coated area, (b) top view. Dark regions correspond to troughs and light regions, to peaks.
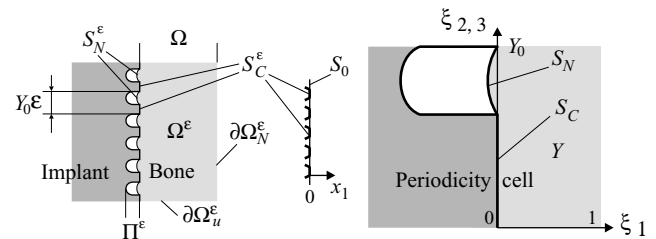

Fig. 2. Contact domains and some notations.

containing the peaks of D^ε (Fig. 2); the volume of $(\Omega^\varepsilon \cup D^\varepsilon)\backslash(\Omega \cup D)$ tends to zero as $\varepsilon \rightarrow 0$.

Let $x = (x_1, x_2, x_3)$ and $\hat{x} = (x_2, x_3)$ be the coordinates of a point in $\mathbb{R}^3$ and those of a point at the plane $x_1 = 0$. For the periodicity cell Y, we introduce the local coordinates ξ that are related to x by $x = \varepsilon \xi$ and denote by T the cross-section of the periodicity cell by a plane $\xi_1 = $ constant, i.e., $T = \{\xi : 0 < \xi_j < Y_0, \quad j = 2,3\}$. The other notation should be clear from Fig. 2.

We consider the case where the domains are bounded and periodic contact conditions are imposed. For the elastic solids occupying the domains Ω^ε and D^ε, denote by $\sigma_{ij}^\varepsilon(x)$ the stress tensor, $u_i^\varepsilon(x)$ the displacement vector,

and $a_{ijkl}(x)$ the symmetric fourth-order tensor of elastic constants at a point $x \in \Omega^{\varepsilon} \cup D^{\varepsilon}$ ($a_{ijkl}(x) = a_{ijkl}^{\Omega}$ if $x \in \Omega^{\varepsilon}$ and $a_{ijkl}(x) = a_{ijkl}^{D}$ if $x \in D^{\varepsilon}$); $i, j, k, l = 1,2,3$.

As is usual in contact problems (see Chapter 6 in Ref. [22]), the contact surfaces are generally unknown, which makes the problem nonlinear, and have to be determined in the course of the solution of the problem. Denote the unknown micro-contact surfaces by $S_{C}^{\Omega^{\varepsilon}}$ and $S_{C}^{D^{\varepsilon}}$ and their projection on the plane $x_1 = 0$ by S_{C}^{ε}.

Following Refs. [22,18], we write out the equilibrium equations and constitutive elastic relations with contact and boundary conditions:

$$\frac{\partial \sigma_{ij}^{\varepsilon}(x)}{\partial x_j} = f_i(x), \; \sigma_{ij}^{\varepsilon}(x) = a_{ijkl}\frac{\partial u_k^{\varepsilon}(x)}{\partial x_l}, \; x \in \Omega^{\varepsilon} \cup D^{\varepsilon}, \tag{1}$$

$$u_n^{R\varepsilon}(x) \leq g^{\varepsilon}(x), \; \sigma_n^{\varepsilon}(x) \leq 0, \; \sigma_n^{\varepsilon}(x)(u_n^{R\varepsilon}(x) - g^{\varepsilon}(x)) = 0, \; x \in S_C^{\varepsilon},$$

$$|\sigma_{i\tau}^{\varepsilon}(x)| < \mu_i(u_{\tau}^{\varepsilon})|\sigma_n^{\varepsilon}(x)| \Rightarrow u_{i\tau}^{R\varepsilon} = 0, \; x \in S_C^{\varepsilon}, \tag{2}$$

$$\sigma_{i\tau}^{\varepsilon} = -\mu_i(u_{\tau}^{\varepsilon})|\sigma_n(u^{\varepsilon})|\frac{u_{i\tau}^{\varepsilon}}{|u^{\varepsilon}|} \Rightarrow \exists \lambda \geq 0 \; such \; that \; u_{i\tau}^{R\varepsilon} =$$

$$-\lambda\sigma_{i\tau}^{\varepsilon}, \; x \in S_C^{\varepsilon},$$

$$\sigma_{ij}^{\varepsilon}n_j(x) = t_i(x), \quad x \in \partial\Omega_N^{\varepsilon} \cup \partial D_N^{\varepsilon}; \quad u_i^{\varepsilon}(x) \tag{3}$$

$$= g_{i0}(x), \quad x \in \partial\Omega_u^{\varepsilon} \cup \partial D_u^{\varepsilon}.$$

Here, $\sigma_n^{\varepsilon}(x) = \sigma_{ij}^{\varepsilon}(x)n_j^{\varepsilon}(x)n_i^{\varepsilon}(x)$ is the normal stress, $\sigma_{i\tau}^{\varepsilon}(x) = \sigma_{ij}^{\varepsilon}(x)n_j^{\varepsilon}(x) - \sigma_n^{\varepsilon}n_i^{\varepsilon}(x)$ are the components of the tangential stress vector, $u^{R\varepsilon}(x) = u^{\varepsilon}(x)|_{S_C^{D\varepsilon}} - u^{\varepsilon}(x)|_{S_C^{\Omega\varepsilon}}$, $u_n^{R\varepsilon}(x) = u_i^{R\varepsilon}(x)n_i(x/\varepsilon)$ is the jump in the normal displacement, $u_{i\tau}^{R\varepsilon}(x) = u_i^{R\varepsilon}(x) - u_n^{R\varepsilon}n_i^{\varepsilon}(x)$ are the jumps in the tangential displacements, μ is the friction coefficient ($\mu = 0$ in the case of pure sliding), $n_i^{\varepsilon}(x) = n_i(x,x/\varepsilon)$ are the components of the unit outward normal to the contact interface (more precisely, to the boundary $S_C^{D\varepsilon}$), $g^{\varepsilon}(x) = g(x,x/\varepsilon)$ is the initial gap between the contacting surfaces, g_{i0} and t_i are the components of the prescribed boundary displacement and traction vectors; the Latin subscripts assume the values from 1 to 3.

Relations (1)–(3) represent the strong formulation of the problem, which applies to smooth domains as well as smooth elastic coefficients and right-hand side functions (prescribed volume forces, boundary displacements, and tractions). Since we treat nonsmooth domains and allow nonsmooth functions and intend to adopt the finite element method for numerical solution, the problem is to be rewritten in a weak (variational) formulation.

2.2. Variational formulation

Following Refs. [20,22,23], rewrite relations (1)–(3) in the variational formulation: minimize the functional

$$I^{\varepsilon,\delta}(v) = \frac{1}{2}\int_{\Omega^{\varepsilon} \cup D^{\varepsilon}} a_{ijkl}\frac{\partial v_k(x)}{\partial x_l}\frac{\partial v_i(x)}{\partial x_j}\mathrm{d}x$$

$$+ \frac{1}{2\delta}\int_{S_C^{\varepsilon}} b\left(\hat{x},\frac{x}{\varepsilon}\right)[v_n^R(x) - g^{\varepsilon}(x)]_+^2 \, \mathrm{d}s \tag{4}$$

$$+ \int_{S_C^{\varepsilon}} G_i^{\varepsilon}(x)|v_{i\tau}^R(x)|\mathrm{d}s - \int_{\Omega^{\varepsilon} \cup D^{\varepsilon}} f_i(x)v_i(x)\mathrm{d}x$$

$$- \int_{\partial\Omega_N^{\varepsilon} \cup \partial D_N^{\varepsilon}} t_i(x)v_i(x)\mathrm{d}s$$

for any admissible test functions $v_i(x)$, where $G_i^{\varepsilon}(x) = \mu_i(u_{\tau}^{\varepsilon})|\sigma_n(u^{\varepsilon})|$ is the friction force, $[\cdot]_+ = \max\{0,\cdot\}$, and b and δ are positive penalty parameters, which correspond to the normal contact stiffness and the contact fibre length in the Winkler theory of elastic foundation, respectively.

2.3. Homogenisation procedure

Since relations (1)–(3), as well as its variational formulation (3), have two different size scales on the micro- and macrolevels, it is very difficult to perform its direct numerical solution. Here, it is intended to reduce the problem to a single-scale problem with special interest being given to the effective contact parameters that will arise. For the scale reduction, asymptotic homogenisation was chosen.

The notion of two-scale convergence is adopted, which is understood in the following sense (see Refs. [19,21] for details).

Defintion 1. A sequence of functions $u^{\varepsilon} \in L^2(\Omega)$ is said to be two-scale convergent to a limit $u_0(x,\xi) \in L^2(\Omega \times Y)$ if and only if for any function $\psi(x,\xi) \in \mathscr{D}(\Omega, C_{\mathrm{per}}^{\infty}(Y))$, we have

$$\lim_{\varepsilon \to 0}\int_{\Omega} u^{\varepsilon}(x)\psi\left(x,\frac{x}{\varepsilon}\right)\mathrm{d}x \tag{5}$$

$$= \frac{1}{|Y|}\int_{\Omega}\int_Y u_0(x,\xi)\psi(x,\xi) \, \mathrm{d}x \, \mathrm{d}\xi.$$

The second and third terms in Eq. (4) are of primary interest, since they are contact terms. By the homogenisation of the second term, expressions are obtained of the macroscopic normal and tangential contact stiffnesses. The homogenisation of the third term results in an effective friction force (friction coefficient). Omitting technical details here, the expressions of the effective parameters just mentioned—normal contact stiffness k_n, tangential contact stiffness k_{τ}, and friction force $G_{j\tau}^0$ — are given:

$$k_n = -\frac{1}{|T|}\int_{S_C^{\mathrm{act}}} k^{\varepsilon}(\hat{x},\hat{\xi})\beta_1^2(\xi) \, \mathrm{d}s_{\xi}, \tag{6}$$

$$k_{\tau} = -\frac{1}{|T|}\int_{S_C^{\mathrm{act}}} k^{\varepsilon}(\hat{x},\hat{\xi})\hat{\beta}^2(\xi) \, \mathrm{d}s_{\xi}, \tag{7}$$

$$G_{j\tau}^0(\hat{x}) \leq \frac{1}{|T|}\int_{S_C^{\mathrm{act}}} G_i(\hat{x},\hat{\xi})|\alpha_{j+1}^{(i)}(\xi)|\mathrm{d}s_{\xi}, \tag{8}$$

(a)

$u_n = \mathbf{u}\cdot\mathbf{n} \leq 0$
$u_\tau = \mathbf{u}\cdot\boldsymbol{\tau} = 0$

(b)

$\mathbf{u}\cdot\boldsymbol{\alpha}_1 \leq 0$
$\mathbf{u}\cdot\boldsymbol{\alpha}_2 \leq 0$

(c)

$\mathbf{u}\cdot\boldsymbol{\alpha}(\xi) \leq 0$
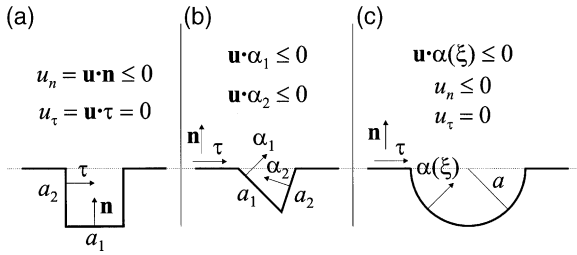$u_n \leq 0$
$u_\tau = 0$

Fig. 3. Periodic microgeometry patterns of the stem surface: (a) rectangular trough, (b) triangular trough, (c) circular trough.

where $|T|$ is the area of the reference contact surface; S_C^{act} is the actual contact surface; $i = 1,2,3$; $j = 1,2$; $k^\varepsilon = b/\delta$; $\alpha_j^{(i)}(\xi)$ is the ith direction cosine of the jth tangent unit vector to the micro-contact surface with respect to the macro-coordinate system; and β_1 and $\hat{\beta}$ are the coefficients in the decomposition of the micro-normal $\mathbf{n}$: $\mathbf{n}(x,\xi) = \beta_1(\xi)\mathbf{n}^0(x) + \hat{\beta}(\xi)\hat{\tau}^0(x)$, $\hat{\tau}^0 = (\tau_1^0, \tau_2^0)$, and $\mathbf{n}$, τ_1^0, and τ_2^0 are the macro-normal and macro-tangents.

2.4. A full contact example

To illustrate the results just presented, consider three 2D cases of various types of trough shown in Fig. 3. We assume that $b = $ constant, $g_0 = 0$, and the surfaces are in full contact (i.e., S_C^{act} coincides with S_C). Denote by $\alpha(\xi)$ both the outward micro-normal and the angle between this vector and the macro-normal. Table 1 presents the normal (k_n) and tangential (k_τ) contact stiffnesses for the three interface microgeometries shown in Fig. 3:

Let us note a few special cases.

(i) In the first case (Fig. 3a), the normal macro-contact stiffness k_n always coincides with the micro-contact stiffness $k^\varepsilon = b/\delta$. The tangential contact stiffness k_τ increases with the depth a_2 of the trough.

(ii) In Fig. 3b, in the limit case of no trough, $\alpha_1 = \alpha_2 = 0$, or a trough with vertical walls, $\alpha_1 = \alpha_2 = \pi/2$, the macro-contact stiffness k_n coincides with the micro-contact stiffness b/δ, as one should expect. In all other cases, k_n is somewhat lower than k^ε; in particular, it can be as low as $(1/2)kn^\varepsilon$ at $\alpha_1 = \alpha_2 = \pi/3$ and $a_1 = a_2 = L$. It is apparent that k_τ increases from zero as the pit depth increases.

(iii) For a semicircle (Fig. 3c), again $k_n = k^\varepsilon$ in the limit case $a = 0$ and $k_n < k^\varepsilon$ in all other cases, attaining its minimum $(\pi/4)k^\varepsilon$ at $a = (1/2)L$. The value of k_τ increases from zero to $(\pi/4)k^\varepsilon$ with a.

(iv) It is interesting to compare the values of k_n for the three different types of pits having the same depth h. For example, if $h = (1/4)L$, we have (a) $k_n = k^\varepsilon$, (b) $k_n = (7/8)k^\varepsilon$ (minimum), and (c) $k_n = ((4 + \pi)/8)k^\varepsilon$.

2.5. Partial plane contact with known contact area

With the assumption that all micro-peaks have plane summits, and thus the contact surface is plane, a simple formula is obtained for the homogenised contact stiffness k_n,

$$k_n(\hat{x}) = \frac{1}{|T|}\int_{S_C^{act}} k^\varepsilon(\hat{x},\xi)\,ds_\xi. \tag{9}$$

In particular, it follows that if $k^\varepsilon = $ constant, the characteristic dimensions of the periodicity cell is $|T| = L$, then

$$k_n = k^\varepsilon |S_C^{act}|/L^2. \tag{10}$$

It also follows that, assuming for rough estimates that all micro-peaks have plane summits with initial contact area of about 0.1–0.2, the periodicity cell cross-section, the effective (homogenised) normal contact stiffness k_n can increase 5–10 times during bone ingrowth from initial partial contact to final full contact, after bone has completely filled the pores in the implant coating and mineralised.

For accurate calculations, it is required to solve a non-linear contact problem for the periodicity cell or every single peak to find the actual contact area and other characteristics. This procedure is not presented here (this is an iterative procedure that involves several computational steps); it will be given elsewhere.

3. Numerical results

3.1. Configuration and parameters

To illustrate and validate the results obtained theoretically, a simplified axisymmetric model was analysed numerically. The aim is to verify that the effective parameters obtained affect the strength of the bone–implant interface and can be used to predict the behaviour of

Table 1

Contact stiffness	Rectangle	Triangle	Semicircle
$k_n/(b/\delta)$	1	$1-(1/L)\Sigma_{i=1}^2 a_i(1-\cos\alpha_i)\cos\alpha_i$	$1-((4-\pi)/2)(a/L)$
$k_\tau/(b/\delta)$	$(1/L)a_2$	$(1/L)\Sigma_{i=1}^2 a_i\sin^2\alpha_i$	$(\pi/2)(a/L)$

$L = |T|$ is the length of the periodicity cell.

actual bone–implant designs taking into account the effect of secondary stability.

We consider a bone–implant configuration where the bone is modelled by a hollow cylinder, fully clamped at the base, with a conical hole for a conical stem with rounded end to avoid stress singularities at the corners; see Fig. 4b. Such a stem models the most important part of a real "conical" stem (see Fig. 4a). The angle of taper of the model stem was taken to be slightly less than that of the real stem to provide higher micromotions at the interface, thus giving an upper estimate for real micromotions. The materials were taken to be isotropic and linear elastic with Young's moduli E_{stem} = 105 GPa (titanium stem) and E_{bone} = 14 GPa (cortical bone). Poisson's ratios were assumed identical and equal to 0.3. The geometric dimensions are shown in Fig. 4b. A series of surface-to-surface large-displacement asymmetric contact analyses was undertaken using the finite element software ANSYS.

An axisymmetric quadrilateral eight-noded finite element was used with target elements on the exterior surface of the stem and contact elements on the interior of the conical hole in the bone. The finite element mesh is shown in Fig. 4c. The values of most of the contact parameters that influence the accuracy of the computation were chosen by default. The penetration tolerance was decreased to 0.01. The normal contact stiffness k_n was varied between 100 and 10 000 GPa/m, and the friction coefficient between 0.1 and 0.6. For full contact, the normal contact stiffness is evaluated as $k^\varepsilon = E_{\text{bone}}/\delta$, where δ is the so-called thickness of the contact layer, which can be estimated as δ = 1–5 mm, and hence k^ε = 2800–14 000 GPa/m. Initially, the contact area can be fairly small—about one tenth of the full contact area in projection onto the macro-surface of contact, so the effective contact stiffness is estimated as $k_n = 0.1k^\varepsilon \approx$ 280–1400 GPa/m. The tangential contact stiffness was

Fig. 4. Axisymmetric macro-model: (a) a typical "conical" stem, (b) model bone–stem configuration, (c) finite element mesh of the model configuration.

found to have no noticeable effect on the results and thus was left default.

3.2. Press-fit simulation

At the first stage, the initial press-fitting of the stem and bone was simulated for various press-fit loads. Fig. 5a shows the settlement of the stem against the press-fit load for two friction coefficients μ = 0.1 and 0.3 and normal contact stiffness k_n = 2000 GPa/m. It is apparent that the settlement is practically linearly dependent on the normal load applied. Fig. 5b illustrates the corresponding number of iterations for the solution to attain the required accuracy. Fig. 5c reveals the effect of the normal contact stiffness k_n on the stem settlement at the press-fit load P = 50 MPa and μ = 0.3. It is shown that the effect becomes weaker as P increases.

3.3. Loading simulation

The same model was then considered with an initial settlement of 5 mm. This settlement was simulated by an initial penetration of 0.2 mm, i.e., the radius of the stem at each point of contact was 0.2 mm greater than the radius of the hole. At this stage, it was important to estimate how the change in the normal contact stiffness k_n and friction coefficient μ affects the interface micromotions, i.e., the relative sliding at the bone–implant interface. A load of 5 MPa was applied to the top face of the stem, which approximately corresponds to 1.5 the patient's weight.

A sensitivity analysis for the maximum sliding and maximum von Mises stress at the interface was carried out in the range of normal contact stiffnesses between 100 and 5000 GPa/m and that of friction coefficients between 0.1 and 0.6. The results are depicted in Fig. 6. As follows from Fig. 6a,b, the effect of k_n on the maximum sliding is significant only for fairly low k_n, i.e., the bone ingrowth effectively increases the interface strength at early stages. Furthermore, an increase in the effective friction coefficient μ leads to a decrease in the maximum sliding, i.e., strengthens the interface.

As far as the maximum von Mises stresses at the interface is concerned, it is quite sensitive to a change in μ and weakly dependent on k_n. This is apparent from Fig. 6c,d.

4. Discussion and conclusions

In cementless surgery, coated-porous implants are used to obtain biological fixation. Bone grows into troughs and pores of an initially press-fitted coated implant within 4–8 weeks and mineralises to provide additional, secondary stability of the implant (e.g., see Refs. [1,3,5,6,8,25]). The effect of secondary stability is
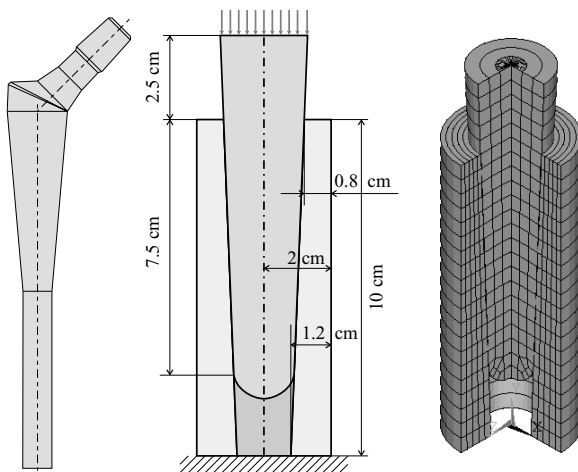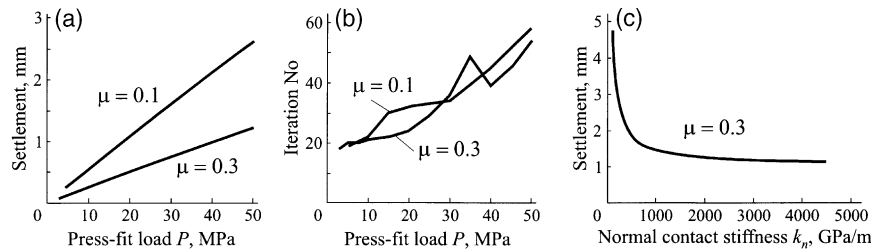
Fig. 5. Press-fit simulation results: (a) settlement vs press-fit load, (b) iteration number to convergence vs press-fit load; $k_n = 2000$ GPa/m; (c) settlement vs normal contact stiffness; $P = 50$ MPa.
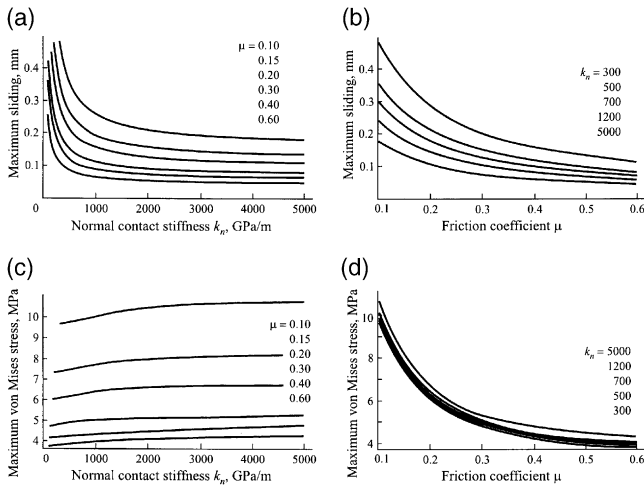

Fig. 6. Sensitivity analysis results: (a) maximum sliding at the interface vs k_n, (b) maximum sliding at the interface vs μ, (c) maximum von Mises stress vs k_n, (d) maximum von Mises stress vs μ. Load applied: $P = 5$ MPa.

absent immediately after the implant has been press-fitted, increases as bone grows into the rough surface of the implant coating, and attains its maximum when bone has completely filled the voids and mineralised.

The study of the bone–stem contact by direct application of the FEM is prohibitively costly. This is because there are two different scales—the micro-size of the peaks and troughs of the coating and the macro-size of the contacting parts of the design. Direct finite element modelling would require millions of finite elements, which is highly prohibitive and, furthermore, does not seem necessary. A natural approach is to simplify the problem by considering the contacting surfaces to be smooth, thus introducing some effective parameters that take into account the interface microgeometry. In this case, the 3D FE modelling would require only tens of thousands of finite elements.

The problem is simplified by the homogenisation of the interface layer, assuming that the stem surface has equal and periodically arranged micro-peaks on some portion of the macro-interface. The mathematical analysis provided us with homogenised parameters, the most important of them being the normal contact stiffness and the friction force (friction coefficient). These parameters

are not constant over the interface and increase as the bone grows into the rough surface of the implant and the effective contact surface increases. Higher values of these parameters increase the interface strength, decrease relative micromotions, and provide for enhanced stability and rapid osseointegration.

One of the problems in designing cementless hip implants and providing their stability is to reduce relative micromotions at the interface to an acceptable level of 50–200 μm. It is reported by many researchers (e.g., see Refs. [4,11,25,26]) that higher micromotions can inhibit bone ingrowth and lead to a fibrous membrane forming between the bone and implant, thus resulting in a mechanically unstable implant. Too low micromotions decrease the rate of bone ingrowth. The above two effective parameters give a tool to control micromotions in FE analyses.

The normal contact stiffness and the friction coefficient can increase several times during the bone ingrowing and mineralisation. In essence, the secondary stability effect arises when bone begins to mineralise. The value of the effective normal contact stiffness is mainly determined by the relative contact area, the ratio of the bone–implant contact area in projection onto the smooth macro-contact surface of contact to the area of the macro-contact surface itself; this ratio is initially about 0.05–0.2 and ultimately about 1. In contrast, the effective friction coefficient is determined by the average slope of peaks on the implant coating; it can be as small as 0.1 initially and can be greater than 1 at late stages (see also Ref. [27]).

Unfortunately, we do not have reliable experimental data at the moment about bone ingrowth and mineralisation processes, which would allow us to establish quantitative laws of change of the effective normal contact stiffness and effective friction coefficient. This issue calls for further investigation.

Acknowledgements

References

[1] Ebramzadeh E, McKellop H et al. Design factors affecting micromotion of porous-coated and low modulus hip prostheses. Trans Orthop Res Soc 1988;13:351–6.

[2] Mirra JM, Marder RA, Amstutz HC. The pathology of failed total joint arthroplasty. Clin Orthop 1982;170:175–83.

[3] Sotereanos NG, Engh CA et al. Cementless femoral components should be made from cobalt chrome. Clin Orthop 1995;313:146–53.

[4] Engh CA, O'Connor D et al. Quantification of implant micromotion, strain shielding and bone resorption with porous-coated anatomic medullary locking prosthesis. Clin Orthop 1992;285:13–29.

[5] Boss JH, Shajrawi I, Mendes DG. The nature of the bone–implant interface. The lessons learned from implant retrieval and analysis in man and experimental animal. Med Prog Technol 1994;20(3-4):119–42.

[6] Kienapfel H, Sprey C et al. Implant fixation by bone ingrowth. J Arthroplasty 1999;14(3):355–68.

[7] Tonino AJ, Therin M, Doyle C. Hydroxyapatite-coated femoral stems. Histology and histomorphometry around five components retrieved at post mortem. J Bone Joint Surg Br 1999;81:148–54.

[8] Søballe K, Hansen ES et al. Tissue ingrowth into titanium and hydroxyapatite-coated implants during stable and unstable mechanical conditions. J Orthop Res 1992;10(2):285–99.

[9] Søballe K. Hydroxyapatite ceramic coating for bone implant fixation. Acta Orthop Scand 1993;64(Suppl 155):1–58.

[10] Søballe K, Toksvig-Larsen S et al. Migration of hydroxyapatite coated femoral prostheses. A Roentgen stereophotogrammetric study. J Bone Joint Surg Br 1993;75(5):681–7.

[11] Søballe K, Hansen ES et al. Hydroxyapatite coating converts fibrous tissue to bone around loaded implants. J Bone Joint Surg Br 1993;75(2):270–8.

[12] Overgaard S, Søballe K et al. Role of different loading conditions on resorption of hydroxyapatite coating evaluated by histomorphometric and stereological methods. J Orthop Res 1996;14(6):888–94.

[13] Hansson S, Norton M. The relation between surface roughness and interfacial shear strength for bone-anchored implants. A mathematical model. J Biomech 1999;32:829–36.

[14] Yosifian GA. Some unilateral boundary value problems for elastic bodies with rugged boundaries. Preprint 99-18 (SFB 359), Heidelberg, 1999.

[15] Jäger W, Oleinik OA, Shaposhnikova TA. Homogenization of solutions of the Poisson equation in a domain perforated along a hypersurface, with mixed boundary conditions on the boundary of the cavities. Trans Moscow Math Soc 1998;59:135–57.

[16] Jäger W, Oleinik OA, Shaposhnikova TA. On homogenization of solutions of the Poisson equation in a perforated domain with different types of boundary conditions on different cavities. Applicable Anal 1997;65:205–23.

[17] Belyaev AG, Piatnitski AL, Chechkin GA. Asymptotic behaviour of a solution to a boundary value problem in a perforated domain with oscillating boundary. Sib Math J 1998;39(4):621–44.

[18] Duvaut G, Lions JL. Inequalities in mechanics and physics. Springer-Verlag, 1976.

[19] Hornung U. Homogenization and porous media. Springer, 1997.

[20] Han W. On the numerical approximation of a frictional contact problem with normal compliance. Numer Funct Anal Optim 1996;17(3-4):307–21.

[21] Allaire G. Homogenization and two-scale convergence. SIAM J Math Anal 1992;23:1482–518.

[22] Kikuchi N, Oden JT. Contact problems in elasticity: a study of variational inequalities and finite element methods. Philadelphia: SIAM, 1988.

[23] Eck C, Jarusek J. Existence results for the static contact problem with Coulomb friction. Math Models Methods Appl Sci 1998;8(3):445–68.

[24] McKoy BE, An YH, Friedman RJ. Factors affecting the strength of the bone–implant interface. In: An YH, Draughn RA, editors. Mechanical testing of bone and the bone–implant interface. CRC Press; 2000. p. 439–62.

[25] An YH, Draughn RA, editors. Mechanical testing of bone and the bone–implant interface. CRC Press; 2000.

[26] Viceconti M, Monti L et al. Even a thin layer of soft tissue may compromise the primary stability of cementless hip stems. Clin Biomech 2001;16:765–75.

[27] Rubin PJ, Rakotomanana RL et al. Frictional interface micromotions and anisotropic stress distribution in a femoral total hip component. J Biomech 1993;26(6):725–39.